

Trends in the magnetic properties of Fe, Co, and Ni clusters and monolayers on Ir(111), Pt(111), and Au(111)

S. Bornemann,^{1,*} O. Šipr,² S. Mankovsky,¹ S. Polesya,¹ J. B. Staunton,³ W. Wurth,⁴ H. Ebert,¹ and J. Minár¹

¹*Department Chemie und Biochemie, Ludwig-Maximilians-Universität München, 81377 München, Germany*

²*Institute of Physics of the ASCR v. v. i., Cukrovarnická 10, CZ-162 53 Prague, Czech Republic*

³*Department of Physics, University of Warwick, Coventry CV4 7AL, United Kingdom*

⁴*Institut für Experimentalphysik, Universität Hamburg and Centre for Free-Electron Laser Science, 22761 Hamburg, Germany*

(Received 27 April 2012; published 28 September 2012)

We present a detailed theoretical investigation on the magnetic properties of small single-layered Fe, Co, and Ni clusters deposited on Ir(111), Pt(111), and Au(111). For this, a fully relativistic *ab initio* scheme based on density functional theory has been used. We analyze the element, size, and geometry specific variations of the atomic magnetic moments and their mutual exchange interactions as well as the magnetic anisotropy energy in these systems. Our results show that the atomic spin magnetic moments in the Fe and Co clusters decrease almost linearly with increasing coordination number on all three substrates, while the corresponding orbital magnetic moments appear to be much more sensitive to the local atomic environment. The isotropic exchange interaction among the cluster atoms is always very strong for Fe and Co exceeding the values for bulk bcc Fe and hcp Co, whereas the anisotropic Dzyaloshinski-Moriya interaction is, in general, one or two orders of magnitude smaller when compared to the isotropic one. For the magnetic properties of Ni clusters, the magnetic properties can show quite a different behavior, and we find in this case a strong tendency towards noncollinear magnetism.

DOI: [10.1103/PhysRevB.86.104436](https://doi.org/10.1103/PhysRevB.86.104436)

PACS number(s): 75.75.Lf, 75.70.Tj, 75.70.Ak

I. INTRODUCTION

The magnetism of surface supported clusters has been the subject of intense research activities over the last few years as such systems often show peculiar and unexpected magnetic behavior. These exceptional magnetic properties arise from the reduced dimensionality in combination with spin-orbit coupling (SOC) that can cause complex interactions among the atomic magnetic moments. In this context, clusters of magnetic *3d* transition metal elements deposited on *5d* noble metal substrates are very interesting as for these systems spin-orbit driven effects mediated by substrate atoms with large SOC are most prominent. With technical or chemical applications in focus, there is a growing need to understand the trends and principles behind the manifold of magnetic properties for different cluster and substrate materials as only this will make it possible to anticipate which magnetic properties may result from a particular cluster/substrate combination.

In previous experimental and theoretical investigations on the magnetism of atomic clusters on surfaces, it was already demonstrated that their magnetic properties differ strongly from the magnetic properties of the corresponding bulk materials and that this has its main origin in the reduced atomic coordination of cluster sites, which, in fact, has a strong impact on the local spin and orbital magnetic moments.¹⁻⁴ More recently, it was also shown that for *3d* clusters or monolayers on *5d* metal surfaces SOC induced effects on the spin configurations also play an immanent role causing various noncollinear magnetic structures.⁵⁻⁷ This SOC induced noncollinear magnetism is, however, intrinsically different from the spin frustrations that may arise, e.g., by a competition between ferro- and antiferromagnetism or that may be present in systems where the magnetic and geometric symmetries are incompatible.^{8,9}

Unfortunately, each of the theoretical studies published so far were aimed at only one or two combinations of the

cluster and substrate materials and often only very few cluster sizes and shapes were investigated. In addition to that comes the fact that many theoretical investigations have focused only on some selected magnetic properties as for instance the magnetic moments and exchange interaction but leaving out important information concerning the magnetic anisotropy energy (MAE). Moreover, due to limitations, which are present in all theoretical schemes, it is often also problematic to compare results obtained for different systems by different groups that use different methods. Thus, in order to obtain a more complete picture about the trends in the magnetic properties of deposited clusters, one needs a sufficiently large self-contained set of results for interrelated systems that are obtained by the same method. This motivated us to calculate a large spectrum of the magnetic properties for sets of Fe, Co, and Ni clusters of 1–7 atoms on Ir(111), Pt(111), and Au(111) surfaces, within a unified fully relativistic Green's function formalism. Moreover, we studied also complete monolayers as reference systems for the sequences with increasing cluster size. This enables us to analyze a large pool of data that are directly comparable because they were obtained by the same procedure. We found that the magnetism of Fe and Co clusters on all investigated surfaces follows common patterns that can be understood by considering the coordination numbers of atoms in the clusters and the polarizability of the substrate. For Ni clusters, the situation is more complicated and some of the systematic trends observed for Fe and Co clusters are absent.

II. COMPUTATIONAL FRAMEWORK

The calculations for the investigated cluster and monolayer systems were done within the framework of spin density functional theory (SDFT) using the local spin density approximation (LSDA) with the parametrization given by Vosko, Wilk,

and Nusair for the exchange and correlation potential.¹⁰ The electronic structure has been determined in a fully relativistic way on the basis of the Dirac equation for spin-polarized potentials, which was solved using the Korringa-Kohn-Rostoker (KKR) multiple scattering formalism.¹¹ The calculations for surface deposited clusters consist of two steps. First, the host surface is calculated self-consistently with the tight-binding or screened version of the KKR method¹² using layers of empty sites to represent the vacuum region. This step is then followed by treating the deposited clusters as a perturbation to the clean surface with the Green's function for the new system being obtained by solving the corresponding Dyson equation.¹³ This technique avoids the spurious interactions between clusters, which may occur if a supercell approach is used instead.¹⁴

For all systems discussed below, the cluster atoms were assumed to occupy ideal lattice sites in the first vacuum layer and no effects of structure relaxation were included. The substrates were simulated by finite slabs which contained 37 atomic layers and we used the experimental lattice parameters of 3.84, 3.92, and 4.08 Å for Ir(111), Pt(111), and Au(111), respectively. The surface calculations were converged with respect to \vec{k} -point integration. For the surface Brillouin zones, a regular \vec{k} mesh of 100×100 points was used, which corresponds to 1717 \vec{k} points in the irreducible part of the Brillouin zone. The effective potentials were treated within the atomic sphere approximation (ASA). The occurring energy integrals were evaluated by contour integration on a semicircular path within the complex energy plane using a logarithmic mesh of 32 points. The multipole expansion of the Green's function was truncated at an angular momentum cutoff of $\ell_{\max} = 2$. For selected surface and cluster systems, calculations with $\ell_{\max} = 3$ were also performed, which showed that this causes a more-or-less uniform increase of the local spin moments by 3–5% and of the local orbital moments by 3–10%. This indicates that the systematic trends in the spin and orbital magnetic moments are well described by $\ell_{\max} = 2$.

For the representation of the interatomic exchange interactions, we made use of the rigid spin approximation¹⁵ and mapped the magnetic energy landscape $E(\{\hat{e}_k\})$ onto an extended classical Heisenberg model for all atomic magnetic moment directions $\{\hat{e}_k\}$. The corresponding extended Heisenberg Hamiltonian has the form^{16,17}

$$H = -\frac{1}{2} \sum_{i,j(i \neq j)} J_{ij} \hat{e}_i \cdot \hat{e}_j - \frac{1}{2} \sum_{i,j(i \neq j)} \hat{e}_i \mathcal{J}_{ij}^S \hat{e}_j - \frac{1}{2} \sum_{i,j(i \neq j)} \vec{D}_{ij} \cdot [\hat{e}_i \times \hat{e}_j] + \sum_i K_i(\hat{e}_i), \quad (1)$$

where the exchange interaction tensor has been decomposed into its conventional isotropic part J_{ij} , its traceless symmetric part \mathcal{J}_{ij}^S , and its antisymmetric part \mathcal{J}_{ij}^A , which is given in terms of the Dzyaloshinski-Moriya (DM) vector \vec{D}_{ij} . We calculated the J_{ij} coupling parameters and DM vectors \vec{D}_{ij} following the scheme by Udvardi *et al.*¹⁷

The anisotropy constants $K_i(\hat{e}_i)$ account for the on-site magnetic anisotropy energy associated with each individual magnetic moment oriented along \hat{e}_i . The magnetic anisotropy energy ΔE is usually split into two parts, the SOC induced

magnetocrystalline anisotropy ΔE_{soc} and the so-called shape anisotropy ΔE_{dd} caused by magnetic dipole-dipole interactions, i.e.,

$$\Delta E = \Delta E_{\text{soc}} + \Delta E_{\text{dd}}. \quad (2)$$

ΔE_{dd} can be determined classically by a lattice summation over the magnetostatic energy contributions of the individual magnetic moments or in an *ab initio* way by using a Breit Hamiltonian.¹⁸ Here, we used the classical approach to calculate ΔE_{dd} for the full monolayers, while we found that for clusters containing just a few magnetic atoms ΔE_{dd} is negligible. The magnetocrystalline anisotropy energy ΔE_{soc} was extracted from magnetic torque calculations, which are described in more detail in Refs. 14,19, and 20.

As already discussed previously by many authors, the approximations and truncations mentioned in this section result in a limited accuracy concerning in particular the values of ΔE_{soc} (see, e.g., Refs. 14,21–23, and 24). However, this does not hinder our analysis of the general trends of ΔE_{soc} with respect to cluster geometries as well as different cluster/substrate combinations. Moreover, neglecting structural relaxations and placing the cluster atoms at ideal lattice sites of the underlying substrate provides an adequate frame of reference for studying pure coordination and direct chemical effects.

III. RESULTS AND DISCUSSION

A. Magnetic moments

Figure 1 shows the considered cluster geometries together with the calculated values of local spin (μ_{spin}) and orbital (μ_{orb}) magnetic moments for Fe clusters of 1–7 atoms as well as full Fe monolayers deposited on Ir(111), Pt(111), and Au(111). For identical Co and Ni clusters the corresponding data are presented in Figs. 2 and 3. In addition, these figures also show the induced spin magnetic moments of the respective substrate atoms that are adjacent to cluster atoms. One can see that in some cases there are considerable variations of μ_{spin} and μ_{orb} between the different sites of the deposited clusters. The magnetic moments depend not only on the position of the site with respect to other Fe, Co, or Ni atoms but also on their position with respect to the underlying substrate atoms. This can be observed, for example, when inspecting the two differently located compact trimers or the noncompact five atom clusters in Figs. 1–3. Clusters supported by Pt(111) have largest μ_{spin} when compared with Ir(111) and Au(111), while the μ_{orb} values are increasing from Ir to Pt to Au.

There is a big difference between the induced magnetic moments in the Ir(111) and Pt(111) substrates on the one hand and the Au(111) substrate on the other hand. Ir and Pt atoms that are nearest neighbors of any Fe or Co atom have a relatively large μ_{spin} of up to $0.15 \mu_{\text{B}}$, while the corresponding Au atoms have always small negative μ_{spin} , not larger than $0.03 \mu_{\text{B}}$ in the absolute value. Substrate atoms with a larger number of Fe, Co, or Ni neighbors usually have a larger μ_{spin} than substrate atoms with a smaller number of neighboring cluster atoms. However, this is not a general rule as seen for the substrate atoms adjacent to the central atom of the noncompact Fe₅ and Co₅ or to the differently located compact Fe₃ and Co₃ clusters on Ir(111) and Pt(111).

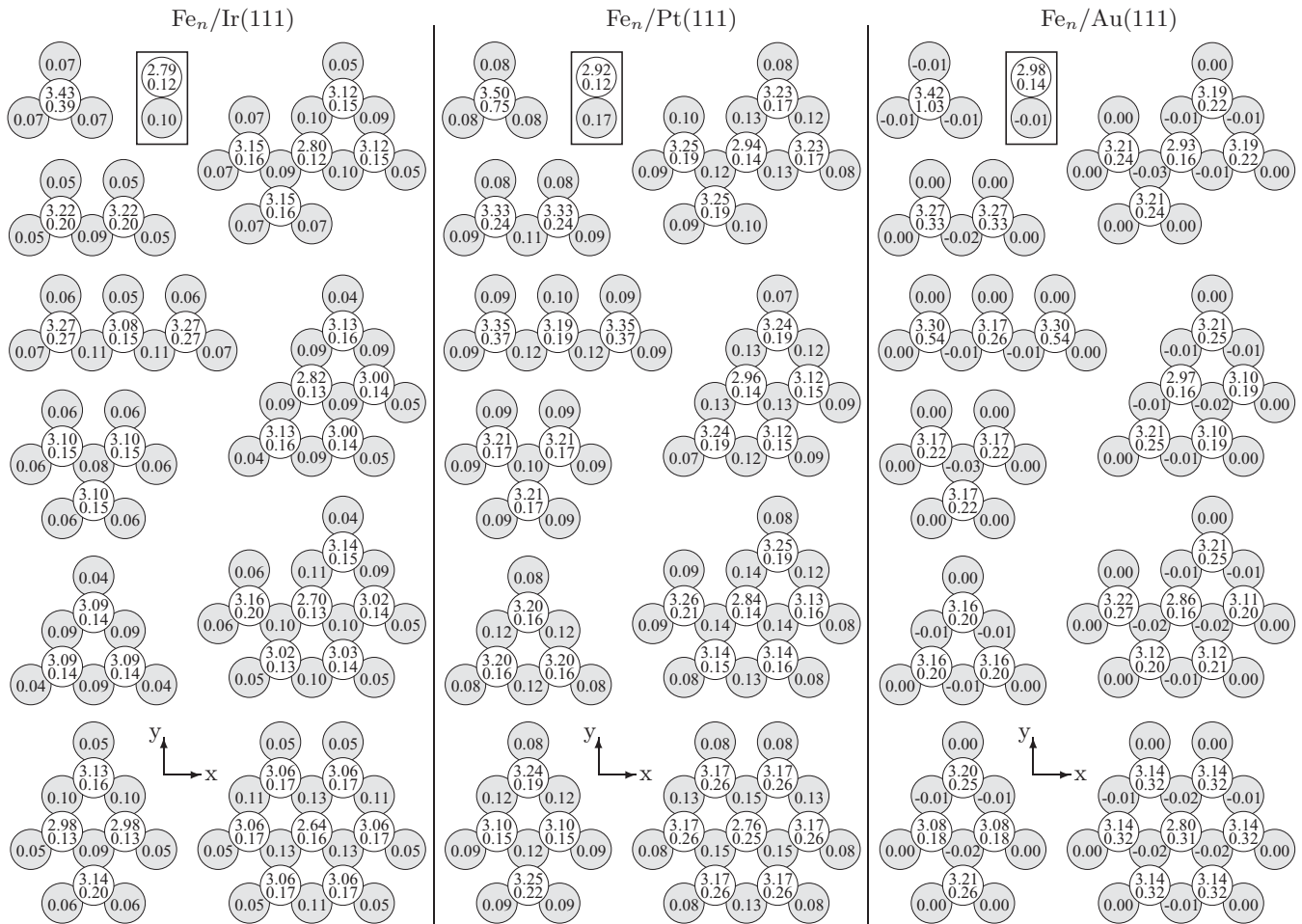


FIG. 1. Cluster geometries for Fe clusters of 1–7 atoms supported by Ir(111), Pt(111), and Au(111). The local spin and orbital magnetic moments at Fe sites are given by the upper and lower numbers, respectively. The spin magnetic moments for nearest-neighbor substrate sites are also shown. The data presented within frames give the corresponding monolayer values.

The orbital magnetic moments induced in the substrate atoms are always small: they can reach up to $0.03 \mu_B$ for Fe and Co on Pt(111), while being smaller than $0.007 \mu_B$ for Ir(111) and smaller than $0.004 \mu_B$ for Au(111). Except for the Au(111) substrate atoms, μ_{orb} is found to be always parallel with μ_{spin} . The finding that Pt is the most polarizable of the three elements and that Au is less polarizable than Ir is consistent with earlier theoretical^{25,26} and experimental works^{27–30} for multilayer systems. This high spin polarizability of Pt can be ascribed to its high spin susceptibility, which in turn is caused by its relatively large density of states at the Fermi level leading to a large Stoner product (see below).

By plotting the local magnetic moments as a function of the coordination number, one can visualize the site-dependence of μ_{spin} and μ_{orb} . Such plots are shown in the insets of Fig. 4, where only neighboring cluster atoms are considered in defining the coordination number. Sites with a lower coordination number generally have larger μ_{spin} and μ_{orb} than sites with a higher coordination number, with Ni on Ir(111) being the only exception. For Ni on Ir(111), the magnetic moments quasioscillate strongly with changing cluster size or shape and we find that μ_{spin} for the adatom ($0.38 \mu_B$) is smaller than for a Ni atom in the full monolayer ($0.49 \mu_B$). For all other

cluster/substrate systems considered in our study, a quasilinear relationship between μ_{spin} and coordination number is found. Interestingly, increasing the coordination number for the atoms of such small clusters leads to a stronger reduction of μ_{spin} when compared to equally coordinated atoms in larger clusters or full monolayers. For example, the central atom of a compact seven-atom cluster has always lower μ_{spin} than a monolayer atom. One can also see that the corresponding orbital magnetic moments are much more sensitive with respect to coordination than the spin magnetic moments. While the insets in Fig. 4 show a strong decay of μ_{orb} with increasing coordination for Fe and Co clusters, on all three substrates the orbital magnetism in Ni clusters behaves nonmonotonously.

An analysis of the average spin and orbital magnetic moments as function of cluster size is shown in Fig. 4. For the three and five atom clusters, the lower μ_{spin} and μ_{orb} values correspond to the compact clusters. All clusters have largest μ_{spin} when deposited on Pt(111) followed by the Au(111) substrate. The lowest μ_{spin} values are obtained for deposition on Ir(111). The highest values of μ_{orb} , however, are found for clusters deposited on Au(111) where the interaction between cluster and substrate atoms is weak and the lattice constant largest.

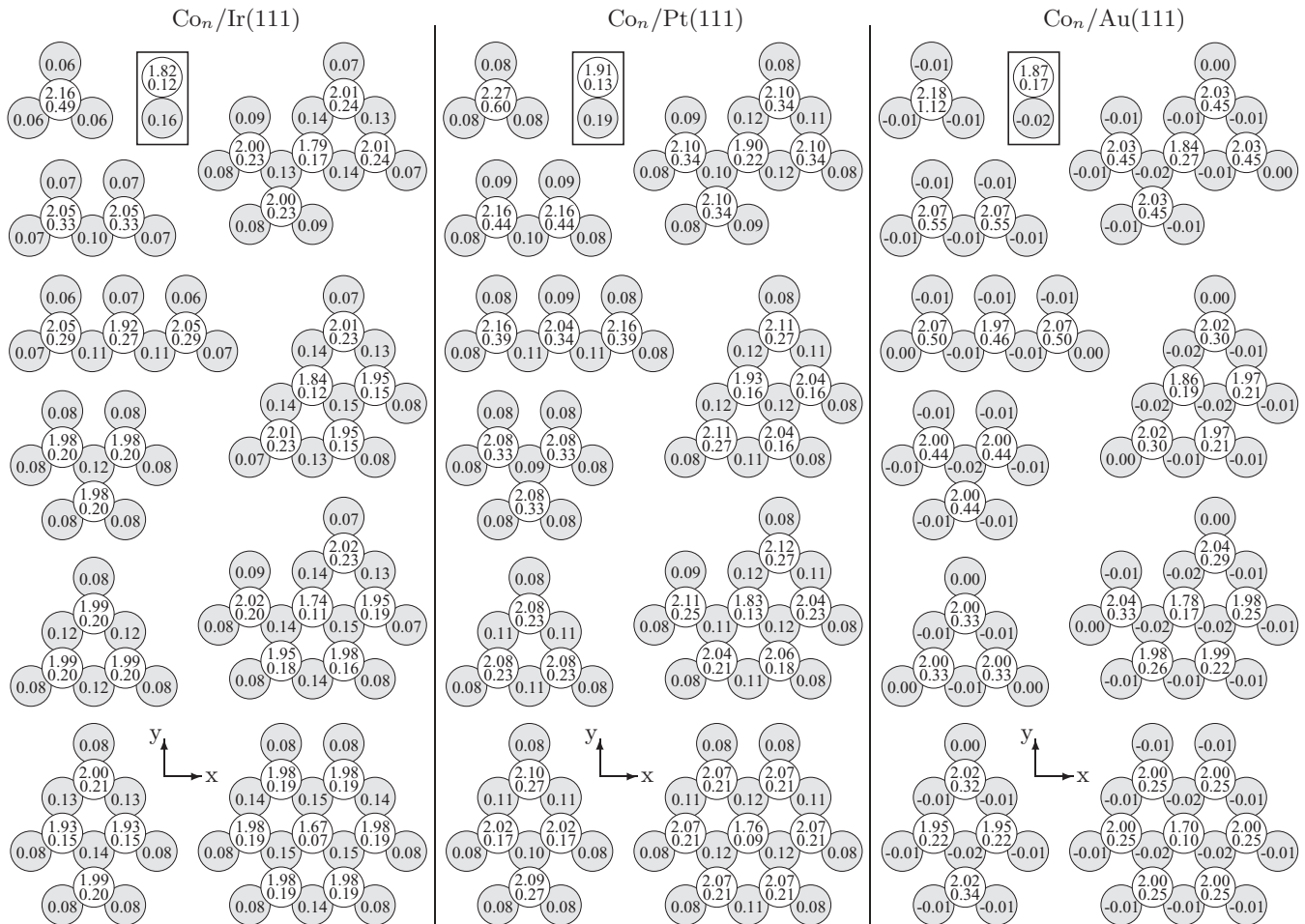


FIG. 2. Cluster geometries for Co clusters of 1–7 atoms supported by Ir(111), Pt(111), and Au(111). The local spin and orbital magnetic moments at Co sites are given by the upper and lower numbers, respectively. The spin magnetic moments for nearest-neighbor substrate sites are also shown. The data presented within frames give the corresponding monolayer values.

Concerning the trend of μ_{spin} for the three different substrates there are two competing effects that must be considered. At first, there is an increase in the lattice constant when going from Ir ($a = 3.84 \text{ \AA}$) to Pt ($a = 3.92 \text{ \AA}$) to Au ($a = 4.08 \text{ \AA}$), i.e., as the atoms of the clusters occupy ideal lattice sites, their distance from the substrate is largest in the case of Au. This means also that among the discussed substrates, the interaction between adatoms and substrate is smallest for Au and one would therefore expect that clusters deposited on Au(111) would have the largest μ_{spin} values. On the other hand, hybridization of the electronic states between adatoms and substrate leads to a small charge transfer of minority $3d$ electrons from the cluster atoms into empty $5d$ states of adjacent substrate atoms, thereby increasing μ_{spin} for the clusters. This, however, happens only for the spatially extended $5d$ states of Ir and Pt with their $5d$ states having an appreciable energetic overlap with the minority $3d$ states of cluster atoms. This can be clearly seen from the density of states curves that are presented in Fig. 5. In contrast to this, there is almost no or only little interaction between the minority $3d$ states of cluster atoms with the energetically low-lying $5d$ states of Au. Besides, the hybridization between the cluster-derived and substrate-derived states leads to energy

lowering of the Fe, Co, and Ni $4p$ states, and this lowering is again more pronounced for the Ir and Pt substrates than for the Au substrate.

This causes an additional charge redistribution within the cluster atoms, i.e., $4p$ states become occupied, again at the cost of minority $3d$ states. In this way, Fe₁ deposited on Pt(111) ends up with about 0.1 electrons less in the minority $3d$ orbitals and thus a slightly larger spin magnetic moment when compared to the deposition on Au(111), with this effect becoming stronger for Co and Ni. Šipr *et al.*³ have demonstrated this behavior for Co clusters on Pt(111) and Au(111) by performing calculations for Co clusters on an Au(111) substrate using the lattice constant of Pt. This also showed that the observed increase in μ_{orb} can be solely attributed to the larger lattice constant of Au.

B. Density of states

In Fig. 5, we show the spin-resolved density of states (DOS) for the adatoms, dimers, and the central atoms of the seven-atom clusters as well as the corresponding full monolayers. The DOS of the respective topmost atomic layer of the clean substrates is also shown by the brown areas together with the

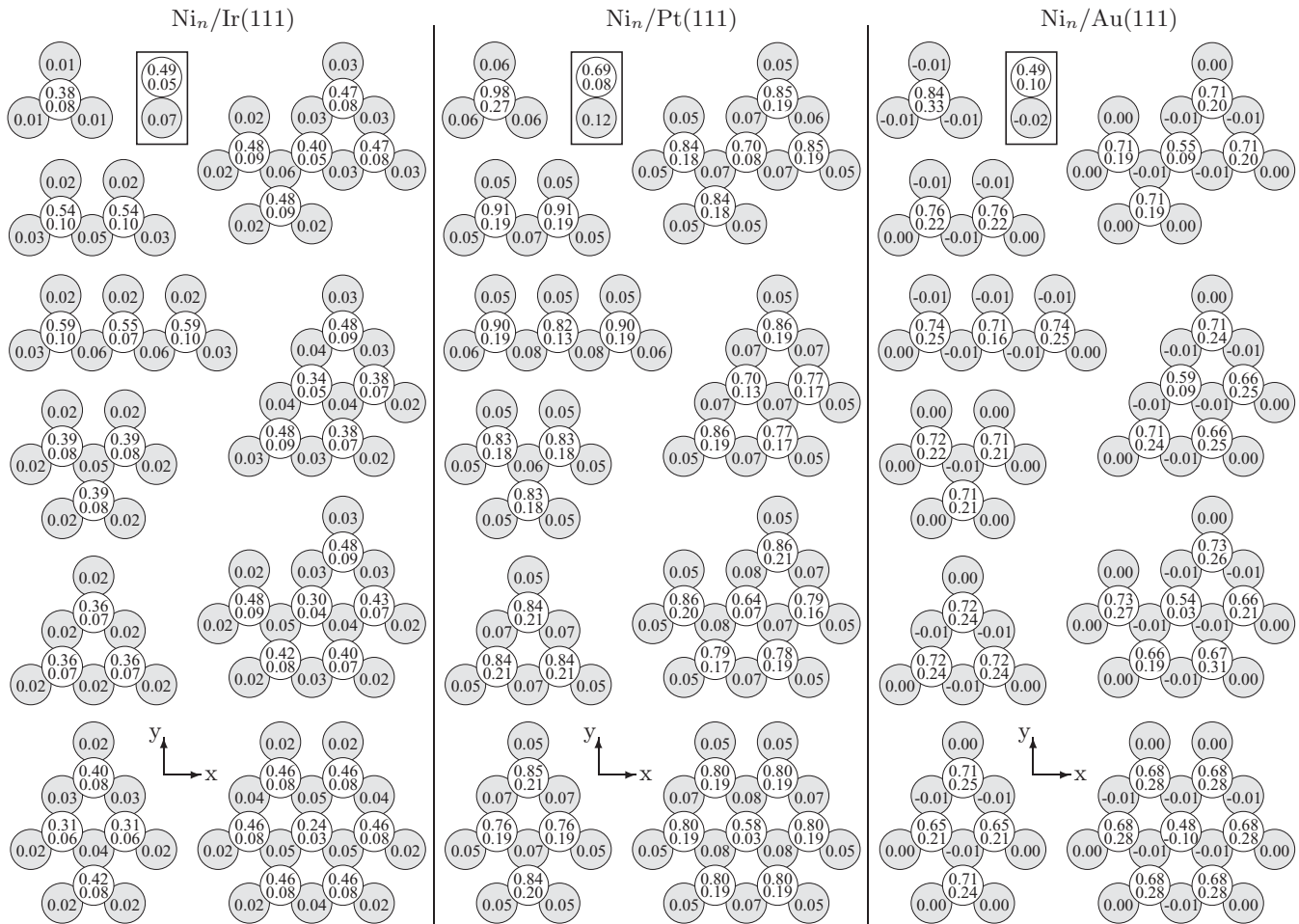


FIG. 3. Cluster geometries for Ni clusters of 1–7 atoms supported by Ir(111), Pt(111), and Au(111). The local spin and orbital magnetic moments at Ni sites are given by the upper and lower numbers, respectively. The spin magnetic moments for nearest-neighbor substrate sites are also shown. The data presented within frames give the corresponding monolayer values.

respective Bloch spectral function $A^B(\vec{k}, E)$ along the high symmetry lines $\bar{\Gamma}-\bar{K}-\bar{M}-\bar{\Gamma}$ in the two-dimensional Brillouin zone presented in the first column. $A^B(\vec{k}, E)$ can be interpreted as a k -resolved DOS revealing the detailed features in the electronic structure of the three different substrates. The large grey-shaded regions in the $A^B(\vec{k}, E)$ diagrams in the first column of Fig. 5 correspond to electronic bulk states of the underlying substrates, while the sharp black lines represent surface states localized within the topmost atomic layer of the clean surfaces. The blue and red regions arise from hybridizations between surface and bulk states. Clearly visible are for instance the Rashba split surface states around $\bar{\Gamma}$ for Pt(111) and Au(111).

For Ir and Pt, there is an appreciable energetic overlap between electronic states located at the substrate and states located at cluster sites resulting in hybridization with a prominent broadening in the cluster DOS. The situation is different for the Au substrate, where the energetically low-lying states of Au can only hybridize with the majority states of Fe while for minority states of Fe as well as for all states of Co and Ni, there are no energetically close Au states to hybridize with and hence very distinct atomic-like features prevail in the DOS of cluster atoms in that case. With increasing

number of cluster atoms, a complex fine structure appears in the DOS that also broadens appreciably with increasing coordination numbers of the cluster atoms. Moreover, the presented DOS curves for the central atom of the seven-atom cluster demonstrate that the DOS of deposited clusters acquires very quickly the main features that are present in the DOS of a complete monolayer. However, as for such small clusters, the DOS at the Fermi level varies strongly with changing the number of atoms, so do the corresponding chemical and magnetic properties in this finite size regime.

The decreasing overlap between states located in the substrate and located in the clusters when going from Ir to Au explains the finding that μ_{orb} is largest for clusters on Au where the atomic-like character of the DOS prevails. In this context, however, the size of μ_{spin} cannot always be directly related to the overlap between cluster and substrate DOS as this overlap is smaller for Au(111) than for Pt(111) and yet μ_{spin} is largest for clusters on the Pt(111) substrate.

In the same way, also the induced magnetization within the substrate depends on this mutual energetic overlap between $3d$ and $5d$ states, which explains the very small induced magnetic moments in the case of Au(111). But also here, one should keep in mind that the polarizability of the substrate atoms is

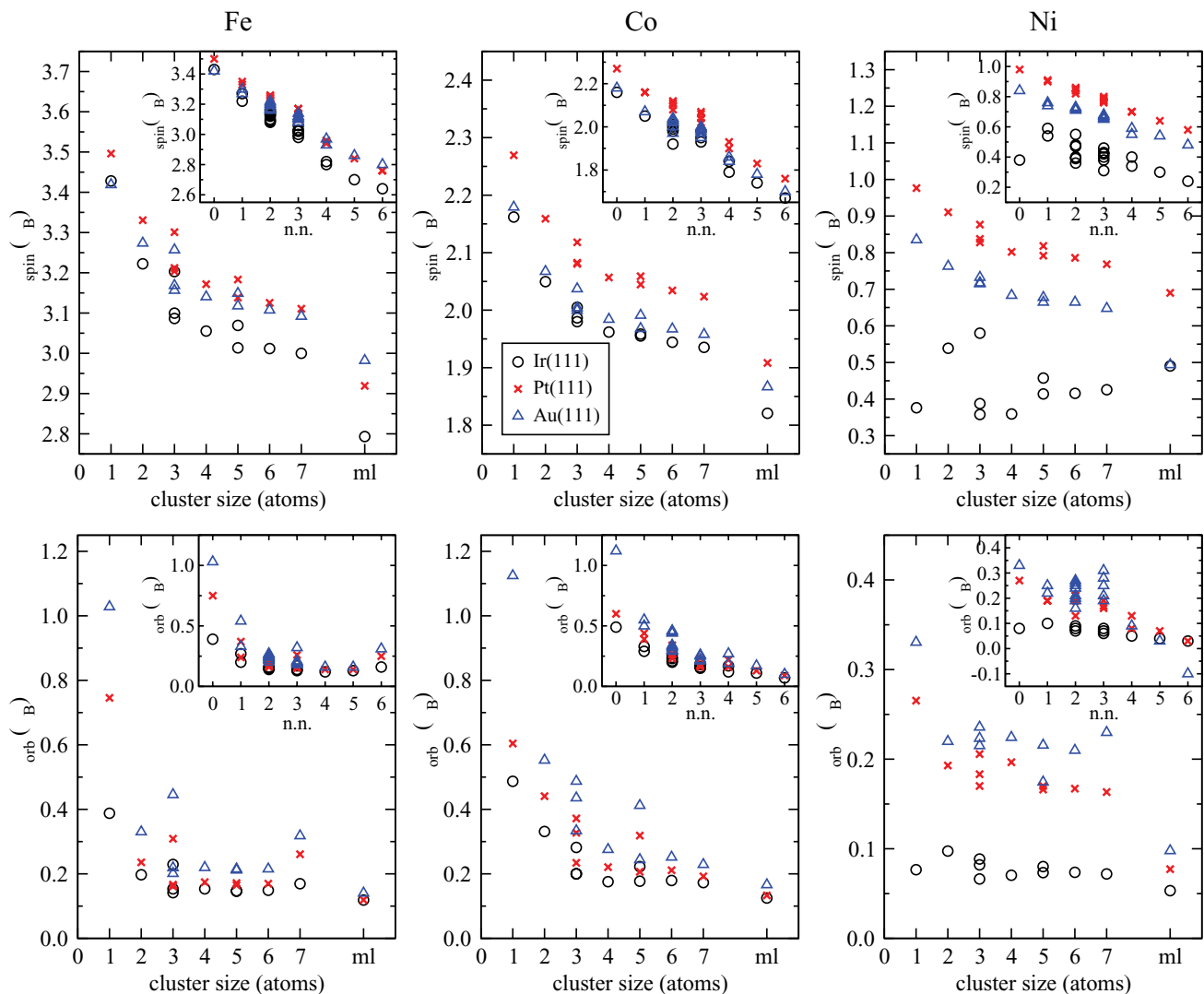


FIG. 4. (Color online) Average spin (top row) and orbital (bottom row) magnetic moments per atom for Fe, Co, and Ni clusters and monolayers (ml) on Ir(111), Pt(111), and Au(111), respectively. The insets present μ_{spin} and μ_{orb} versus the number of nearest neighboring cluster atoms (n.n.).

determined by the Stoner product $I \cdot N_F$ with the exchange integral I and the number of states at the Fermi level N_F ($I \cdot N_F = 0.29$ for Ir, 0.59 for Pt, and 0.05 for Au).³¹

C. Exchange coupling

The calculated isotropic exchange coupling constants J_{ij} are presented for all clusters (except for the noncompact five-atom and six-atom ones) in Table I. Positive and negative values of J_{ij} correspond to ferromagnetic and antiferromagnetic coupling, respectively. In Table II, we show the sum of all couplings related to a particular atom at site i :

$$J^i = \sum_{i \neq j} J_{ij}. \quad (3)$$

The effective exchange field J^i can be seen as the total strength by which the magnetic moment at site i is held along its direction by all other atoms.

From the data given in Table I one can see that Fe and Co clusters show a strong ferromagnetic nearest-neighbor coupling in the range of 40–140 meV, while for Ni clusters the J_{ij} values are often much smaller. In the case of Fe and Co, the couplings between nearest neighboring atoms are about one order of magnitude larger than couplings between more distant atoms, i.e., the coupling strength falls off very rapidly with increasing the interatomic distance. For Ni clusters, however, and especially for Ni on Ir(111) where the couplings are very weak this trend is less pronounced. These results also show that there is an occasional weak antiferromagnetic coupling between more distant atoms for Fe clusters, which, however, gives only an insignificant contribution to the cumulative J^i of each respective atom. As each J_{ij} contains by definition [see the Heisenberg Hamiltonian in Eq. (1)] the product between the involved spin magnetic moments μ_{spin}^i and μ_{spin}^j the coupling is, naturally, largest for Fe and smallest for Ni clusters. Moreover, the nearest-neighbor exchange coupling among the Fe, Co, and Ni cluster atoms is larger than our

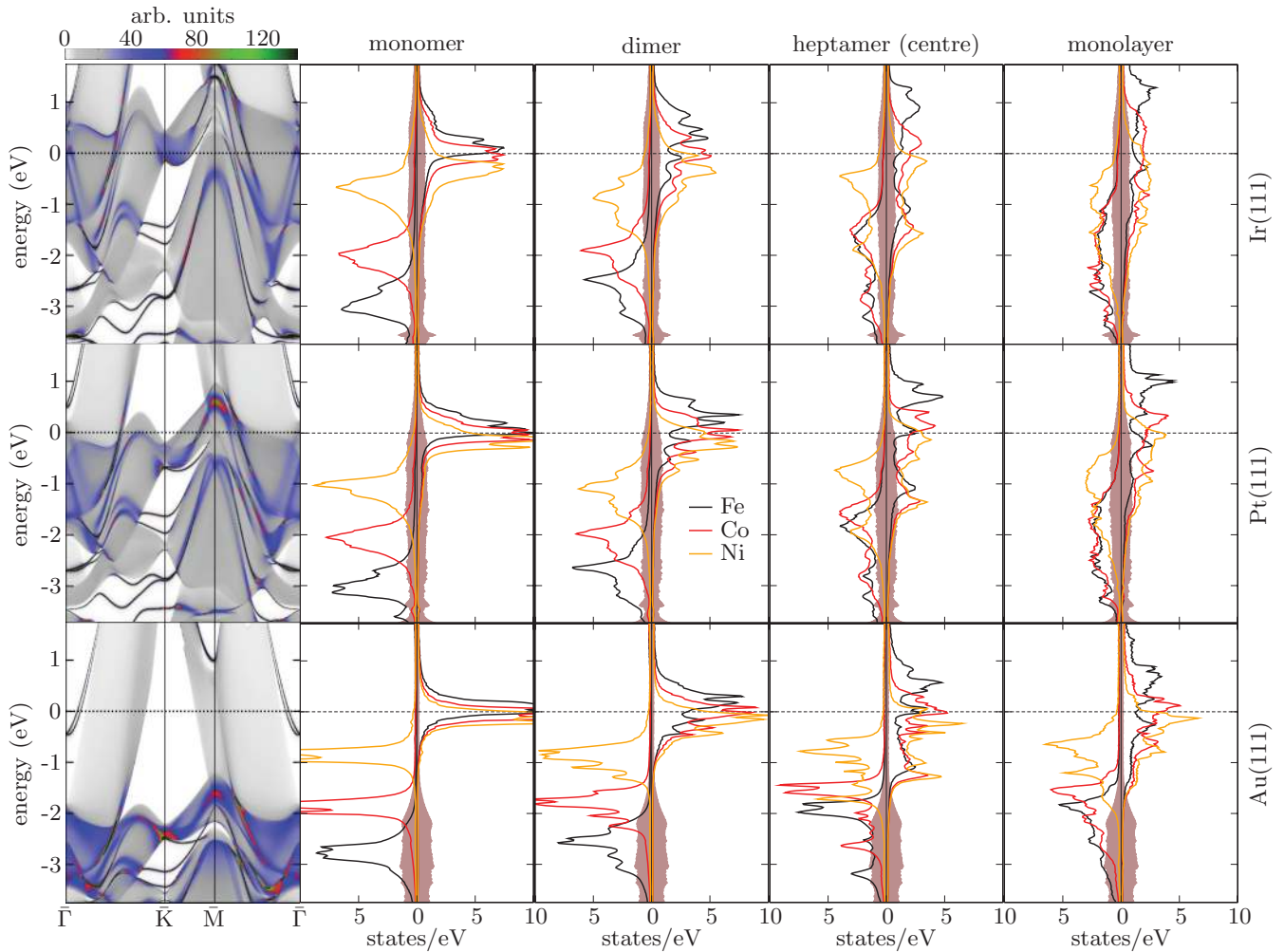


FIG. 5. (Color online) Spin projected density of states (DOS) for Fe, Co, and Ni monomers (second column), dimers (third column) as well as the central atom of a seven-atom cluster (fourth column) and the corresponding full monolayers (rightmost column) deposited on the (111) surfaces of Ir (top row), Pt (middle row), and Au (bottom row) of clean substrates. Corresponding Bloch spectral functions $A^B(\vec{k}, E)$ for surface atoms of clean substrates are presented in the leftmost column along the $\bar{\Gamma}$ - \bar{K} - \bar{M} - $\bar{\Gamma}$ line of the two-dimensional Brillouin zone.

corresponding values for standard bcc Fe (37.8 meV), hcp Co (26.3 meV), and fcc Ni (4.8 meV).





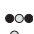
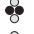
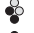













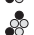

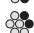
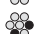


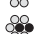
Apart from the magnitude of the spin magnetic moments also atomic coordination as well as substrate effects play an important role. Especially for Fe clusters, the J_{ij} values between low coordinated cluster atoms are often much larger when compared to atoms with higher coordination. Nevertheless, the effective exchange field J^i increases monotonically with increasing coordination, i.e., given a fixed number of Fe, Co, or Ni atoms the most compact structure will form the most stable ferromagnetic state.

As one can clearly see from the data in Table I in combination with the cluster geometries given in Figs. 1–3 the isotropic exchange coupling is also affected by the arrangement of cluster atoms with respect to the underlying surface sites. Looking at the two different compact Fe and Co trimers on Ir(111) and Pt(111), for instance, we find that the coupling values differ by about 8–10%. For the seven-atom Fe cluster on Ir(111) and Pt(111), however, J_{ij} for nearest neighboring edge atoms varies by as much as 20–45%, respectively, whereas

the corresponding couplings for clusters on Au(111) do, in general, not exhibit such a pronounced dependence on the atomic position with respect to the substrate atoms. The latter seems also to be the case for Fe and Co seven-atom clusters with an identical configuration on Cu(111). This was studied in detail by Mavropoulos *et al.*⁴ and the Cu substrate atoms also do not seem to participate in the exchange coupling of the Fe and Co cluster atoms. Therefore we ascribe this substrate effect to the large spin-polarization within the the Ir and Pt surface atoms, while the weak induced magnetism in Cu and Au causes only minor variations in the exchange coupling of equidistant cluster atoms. These irregularities in the couplings underline that transferring J_{ij} coupling constants obtained from bulk calculations to low-dimensional finite nanostructures will lead, in general, to unreliable results.

For Fe and Co clusters, the magnitude of the isotropic exchange interaction is quite similar for all three investigated substrates. Ni clusters, on the other hand, have comparable nearest-neighbor J_{ij} values only when being deposited on Pt(111) and Au(111), while deposition on Ir(111) reduces the

TABLE I. Isotropic exchange coupling constants J_{ij} (meV) for Fe, Co, and Ni clusters deposited on Ir(111), Pt(111), and Au(111). The icons in the left column indicate the corresponding cluster geometry as well as the cluster sites i and j , respectively. The last line gives J_{ij} for nearest neighboring sites within the full monolayer (ml).

ij	Fe			Co			Ni		
	Ir	Pt	Au	Ir	Pt	Au	Ir	Pt	Au
	128.8	137.8	143.8	97.5	107.7	112.8	7.9	30.4	26.7
	110.5	111.8	114.6	69.8	77.6	72.5	0.8	14.6	16.1
	100.3	107.9	114.2	64.5	71.0	67.4	1.8	16.4	15.7
	76.8	90.9	90.6	66.9	76.9	74.8	11.2	24.9	20.9
	-15.9	-8.4	-12.2	5.2	3.9	-0.4	4.3	6.1	3.4
	79.5	79.2	82.3	49.5	59.8	47.5	0.4	7.6	8.0
	83.0	92.1	99.4	59.3	66.1	60.5	2.0	15.9	13.5
	97.2	99.4	100.7	61.4	69.7	60.2	1.4	14.6	12.7
	-1.2	-0.8	-3.8	6.7	8.4	10.1	0.4	3.3	1.6
	79.6	79.2	77.0	53.4	61.5	55.4	3.8	15.1	10.8
	51.2	64.9	67.0	48.4	54.0	46.3	4.2	15.1	10.2
	118.3	117.4	122.2	65.7	69.3	65.1	1.0	16.1	14.0
	109.6	110.2	116.3	66.3	72.2	70.0	2.8	16.7	14.2
	0.7	4.2	5.9	1.5	4.2	6.9	-0.6	1.5	2.2
	-12.4	-7.6	-10.4	4.7	6.2	4.0	2.2	4.9	3.5
	74.2	75.6	75.9	50.3	57.9	45.1	0.8	7.9	7.1
	71.8	79.3	68.8	48.6	53.8	46.2	3.8	16.9	11.7
	67.8	77.1	89.8	45.1	56.0	44.8	3.3	15.1	10.0
	104.0	105.5	105.4	64.0	73.0	65.9	2.1	14.4	9.6
	1.2	0.3	-1.9	3.1	7.9	9.4	0.1	2.4	0.9
	-6.3	-4.4	-4.3	4.0	4.6	5.4	2.1	5.4	3.5
	61.0	72.9	87.9	48.2	59.1	50.8	3.9	13.1	8.8
	88.8	88.1	89.9	50.6	59.4	45.0	3.4	13.1	8.6
	2.4	1.6	2.2	1.0	5.3	7.8	0.4	1.8	0.1
	2.4	1.6	2.2	1.0	5.3	7.8	0.4	1.8	0.1
	-2.4	-0.0	0.7	5.8	6.3	3.0	1.3	3.6	2.5
	57.0	57.2	47.5	38.4	43.7	34.8	1.4	9.1	6.6
ml	34.9	48.9	42.6	33.4	35.7	26.0	3.7	7.7	3.4

coupling strength to just a few milli-electron-volts. This results in a quite small effective exchange field J^i per Ni atom in the order of about 10 meV. As the exchange interaction is so small for these Ni clusters, there is a pronounced tendency that

their magnetic ground state deviates strongly from a collinear configuration (see below).

The coupling of magnetic cluster atoms to the induced magnetic moments in the substrate is always very small. J_{ij} is

TABLE II. Effective exchange field J^i (meV) for Fe, Co, and Ni clusters deposited on Ir(111), Pt(111), and Au(111). The icons in the left column indicate the corresponding cluster geometry as well as the cluster site i . The last line gives J^i for the full monolayer (ml).




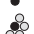
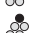
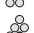




























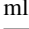
i	Fe			Co			Ni		
	Ir	Pt	Au	Ir	Pt	Au	Ir	Pt	Au
	267.1	297.2	289.6	210.6	236.6	203.8	16.4	62.0	42.1
	190.7	201.3	196.1	131.8	147.4	132.0	6.9	39.8	30.6
	153.8	180.1	180.3	126.6	142.5	128.0	9.1	40.1	30.2
	296.5	317.8	290.8	204.3	228.9	182.9	9.6	51.3	37.7
	174.7	188.9	169.4	126.0	145.7	127.4	8.7	41.3	25.9
	252.1	266.8	271.0	168.6	199.6	165.7	6.7	41.5	27.6
	348.3	351.8	286.3	235.6	267.1	208.9	8.7	55.8	39.9
	215.1	230.2	232.0	151.2	184.6	149.8	11.3	44.5	26.9
ml	205.5	285.4	244.6	227.0	233.5	190.9	27.8	58.5	27.7

TABLE III. Anisotropic exchange coupling parameter $|\vec{D}_{ij}|$ (meV) for Fe, Co, and Ni clusters deposited on Ir(111), Pt(111), and Au(111). The icons in the left column indicate the corresponding cluster geometry as well as the cluster sites i and j , respectively. The last line gives $|\vec{D}_{ij}|$ for nearest neighboring sites within the full monolayer (ml).

ij	Fe			Co			Ni		
	Ir	Pt	Au	Ir	Pt	Au	Ir	Pt	Au
	1.17	6.93	1.61	3.48	5.47	2.34	0.26	0.24	0.49
	4.60	6.16	0.70	1.06	1.17	4.18	0.39	1.45	0.99
	0.94	6.31	2.45	5.76	8.31	8.66	0.24	2.35	1.32
	1.83	5.64	2.77	2.06	3.51	1.27	0.48	0.63	0.48
	3.62	1.19	3.78	0.38	1.79	2.91	0.40	1.20	1.42
	4.86	6.02	1.52	2.29	0.67	1.73	0.14	0.97	1.45
	1.76	5.64	2.26	4.33	4.24	2.85	0.20	1.09	1.57
	2.54	5.30	0.98	1.19	1.39	2.14	0.26	0.28	0.39
	1.58	0.64	0.75	0.34	1.75	0.99	0.09	0.58	0.19
	5.75	5.81	0.63	2.97	6.03	7.98	0.54	0.87	0.26
	2.25	5.12	1.85	4.81	5.63	3.29	0.52	1.42	0.73
	4.67	6.97	2.51	3.43	6.24	5.82	0.51	0.88	0.90
	1.39	5.46	1.45	7.55	9.98	4.72	0.50	1.06	1.48
	1.30	1.03	2.24	0.83	0.80	1.95	0.37	0.63	0.23
	2.34	0.77	0.86	1.40	2.21	3.11	0.16	0.61	0.40
	5.60	5.26	2.00	2.30	1.82	5.39	0.15	0.88	1.21
	3.33	3.64	1.19	1.14	1.47	1.34	0.26	0.54	0.34
	2.51	5.22	1.43	3.83	1.54	3.81	0.39	0.42	1.19
	2.90	4.90	1.21	1.46	2.58	2.40	0.31	0.28	0.76
	0.79	0.35	0.73	0.40	1.73	1.10	0.17	0.40	0.49
	1.49	0.46	1.45	1.12	1.31	1.74	0.35	0.74	0.27
	1.00	4.99	1.08	5.01	1.86	1.99	0.45	0.26	0.72
	3.72	6.00	2.55	1.44	2.88	1.56	0.26	0.23	1.22
	1.28	0.43	0.97	0.57	1.20	0.80	0.10	0.27	0.39
	1.28	0.43	0.97	0.57	1.20	0.84	0.10	0.29	0.38
	0.58	0.43	1.70	1.97	1.56	0.86	0.12	0.33	0.33
	3.81	2.52	2.55	1.48	1.75	1.67	0.13	0.35	0.45
ml	4.17	2.54	0.66	1.33	1.68	0.71	0.13	0.20	0.04











about 2 meV between Fe or Co cluster atoms and topmost layer atoms of an Ir or Pt surface. The small induced moments in the Au(111) substrate couple antiferromagnetically to the cluster atoms. Here, the nearest-neighbor J_{ij} 's are only in the order of 0.1 meV being of similar magnitude as the ferromagnetic coupling of Ni cluster atoms to Ir or Pt surface sites.

In addition to the isotropic J_{ij} coupling constants, Table III shows the complementary data for the anisotropic exchange interaction. For clarity, we present here only the magnitude of the DM vector $|\vec{D}_{ij}|$, which can be seen as a measure of the driving force towards a noncollinear spin configuration. Given the fact that the SOC strength is comparable in Ir, Pt, and Au one can see from the data in Table III that for any given cluster there are often strong variations (without any clear trends) in $|\vec{D}_{ij}|$ upon deposition onto different substrates. As discussed above for the J_{ij} values, we find here an even more pronounced dependence of $|\vec{D}_{ij}|$ on the position of cluster atoms with respect to the underlying substrate atoms and the results show in addition that the relative decay of the DM interaction with increasing interatomic distance is much

weaker when compared to the corresponding isotropic exchange coupling.

Albeit that $|\vec{D}_{ij}|$ is between one or two orders of magnitude smaller than the isotropic exchange coupling, it is not negligible. For Fe_n on Ir(111), we obtain a relatively strong DM interaction which is in accordance with the recent findings of Heinze *et al.*⁷ and of von Bergmann *et al.*³² as well as Deák *et al.*³³ for Fe/Ir(001), which all demonstrate that these systems show a strong tendency towards noncollinear magnetism. Moreover, our results also show large $|\vec{D}_{ij}|$ values for Fe_n and Co_n clusters from which we conjecture that this may also lead to complex magnetic structures within extended Fe and Co nanostructures on these substrates. In fact, the sometimes experimentally observed, unexpected low magnetic moments in Fe- and Co-Pt(111) systems may be caused by this mechanism.^{34,35} For Ni clusters, the DM interaction is always very important with respect to the isotropic exchange coupling as both quantities are often of the same order of magnitude. Thus one can expect the presence of noncollinear magnetic ordering in Ni clusters on all three substrates. It should be

TABLE IV. Magnetic anisotropy energy (MAE) per atom for Fe, Co, and Ni clusters deposited on Ir(111), Pt(111), and Au(111). The icons in the left column indicate the corresponding cluster geometry. The positive (negative) values of the MAE (meV) correspond to an out-of-plane (in-plane) magnetic easy axis. For the full monolayers the total MAE ΔE is decomposed into its dipolar part ΔE_{dd} and its magnetocrystalline part ΔE_{soc} . The latter is further decomposed into contributions that originate from the monolayer ($\Delta E_{\text{soc}}^{3d}$) and the substrate ($\Delta E_{\text{soc}}^{5d}$), respectively. For the deposited clusters, we found $\Delta E_{\text{dd}} \approx 0$ and $\Delta E_{\text{soc}} \approx \Delta E_{\text{soc}}^{3d}$.

	Fe			Co			Ni		
	Ir	Pt	Au	Ir	Pt	Au	Ir	Pt	Au
	0.10	8.42	11.45	3.95	4.88	9.02	-0.21	-1.57	-5.11
	-1.01	0.48	2.75	0.54	2.25	-0.39	0.10	0.08	-1.17
	0.37	0.36	1.33	0.07	-0.12	-2.45	0.84	0.49	0.24
	-0.45	0.33	1.44	1.82	2.00	0.52	0.17	-0.13	-0.62
	-0.07	1.23	3.46	-0.23	0.60	-3.84	0.10	-0.58	3.08
	-0.09	0.36	1.74	0.04	-0.18	-2.56	0.09	0.44	0.15
	-0.49	0.05	1.26	0.74	1.42	-0.03	0.14	0.23	-0.77
	0.11	0.49	1.65	0.17	-0.44	-2.32	0.05	0.21	0.21
	0.09	0.48	1.90	0.36	-0.11	-2.00	0.08	0.22	0.09
	0.90	2.15	3.86	0.30	-0.26	-2.12	0.11	0.37	0.65
					monolayer				
ΔE	0.64	-0.26	1.09	0.20	0.31	-1.32	-0.19	-0.39	-0.44
ΔE_{dd}	-0.19	-0.19	-0.18	-0.09	-0.09	-0.08	-0.01	-0.01	-0.01
ΔE_{soc}	0.83	-0.07	1.27	0.29	0.40	-1.24	-0.18	-0.38	-0.43
$\Delta E_{\text{soc}}^{3d}$	0.82	-0.17	1.27	0.30	0.22	-1.24	-0.19	-0.46	-0.43
$\Delta E_{\text{soc}}^{5d}$	0.01	0.10	0.00	-0.01	0.18	0.00	0.01	0.08	0.00

stressed that this noncollinearity will *not* be a consequence of the frustration between the magnetic and geometric order but rather will follow from the influence of spin-orbit effects on the exchange coupling, as manifested by the DM interaction.

D. Magnetic anisotropy energy

The magnetic anisotropy energies (MAE) per atom for all investigated clusters are compiled in Table IV. Positive MAE values denote an out-of-plane anisotropy, while negative MAE values correspond to an in-plane magnetic easy axis. Fe clusters on Pt(111) and Au(111) show always an out-of-plane MAE, whereas all other cluster substrate systems exhibit a rather nonuniform behavior of their MAE with varying cluster size or geometry. This complex behavior arises from the fact that already tiny changes in the electronic structure can cause large changes in the MAE. This can be seen again for example in the case of the compact trimers where one can observe a dramatic dependence of the MAE on their position with respect to the substrate, i.e., depending on whether a substrate atom is underneath the cluster center or not.

All dimers and linear trimers with in-plane MAE have their magnetic easy axis fixed along the cluster axis which is a result of the strong azimuthal MAE in these systems being in the order of 1–4 meV per atom. For compact symmetric clusters as well as for the full monolayers, there remains only a very small azimuthal MAE in the order of μeV being thus negligible.

When evaluating the MAE by means of the torque method, contributions stemming from all individual atomic sites of the system are added together. One can therefore technically identify which portion of the MAE comes from the adsorbed atoms and which portion comes from the substrate atoms.

We found that the contribution coming from the substrate is negligible in the case of clusters while it can be significant in the case of complete monolayers [e.g., up to 45% of the total value for the Co monolayer on the Pt(111) substrate]. This is plausible given the fact that for monolayers, the substrate atoms are subject to interaction with a larger number of adsorbed atoms, meaning that their spin polarization will be stronger and more robust than in the case of small clusters, contributing thereby more significantly to the MAE. At the same time, one has to bear in mind that energy is not an extensive quantity and that any decomposition of the MAE into parts has only a limited significance.

Concerning the dipole-dipole or shape MAE contribution, for clusters it is negligible while for complete monolayers it attains appreciable values of -0.19 and -0.09 meV per atom for Fe and Co monolayers, respectively. Moreover, we find that the substrate as well as the dipole-dipole contribution to the MAE is negligible for clusters, whereas for monolayers, both contributions are much more important.

E. Comparison with other works

As already mentioned in the introduction it is not always straightforward to directly compare theoretical LSDA results obtained by different computational *ab initio* implementations due to differences in the truncation of the wave function or Green's function, etc., as well as different technical issues and approaches as, for example, the implementation of spin-orbit coupling as perturbation, the use of a supercell versus embedding techniques or approximations in the description of the effective potentials and so forth. All this can affect the obtained numerical results, especially for sensitive magnetic

quantities like, for instance, orbital magnetic moments and magnetic anisotropy energies.

Among the cluster/substrate systems discussed in this article, only Fe_1 and Co_n on Pt(111) have been studied extensively by other groups, and we find for these systems that our spin magnetic moments agree quantitatively well with the corresponding μ_{spin} values given in Refs. 2,22–24,36–38 using identical geometries. The same is true for Fe_3 on Pt(111),⁶ Fe_1 and Co_1 on Ir(111)³⁶ as well as for the monolayer systems Fe/Ir(111),^{32,36} Co/Ir(111),³⁶ Fe/Pt(111), Co/Pt(111),³⁶ and Co/Au(111).³⁹ Regarding the values of μ_{orb} and the MAE, however, the agreement is, in general, less good, i.e., only qualitative or worse, for the above mentioned reasons. As already analyzed by Šipr *et al.*,¹⁴ methods that rely on a supercell approach^{22,24,38} produce always significantly higher induced spin magnetic moments within the substrate atoms when compared to methods that apply embedding techniques.^{2,23,36,37}

IV. SUMMARY AND CONCLUSIONS

The evolution of the spin and orbital magnetic moments of the investigated $3d$ transition metal clusters on $5d$ noble metal surfaces mostly follows common trends and patterns that can be understood by considering the coordination numbers of atoms in the clusters and the polarizability of the substrate. The average μ_{spin} values decrease nearly monotonously with the number of atoms in the cluster being at variance with trends observed for free clusters.⁴⁰ Our results show that

μ_{orb} may strongly depend on the position of the cluster with respect to the surface atoms, as demonstrated in particular for the triangular three-atom clusters on Pt(111) and Au(111). The magnetic moments for Ni clusters on Ir are smaller than one would expect judging from the trends for the other cluster/substrate combinations. Moreover, they depend wildly on number of atoms in the cluster and their smallness is compatible with the fact that the peak in the minority DOS is below E_F .

Apart from $\text{Ni}_n/\text{Ir}(111)$, all clusters show a strong ferromagnetic isotropic exchange coupling exceeding the corresponding bulk values of standard bcc Fe, hcp Co, and fcc Ni. In addition, there are also strong anisotropic DM interactions present revealing the intrinsic tendencies towards noncollinear magnetism in these systems. Finally, the magnetic anisotropy energies can be very large for some cluster/substrate or surface/substrate combinations, but unfortunately, there are no clear trends visible that would allow any straightforward anticipation of this sensitive quantity.

ACKNOWLEDGMENTS

Financial support by the Bundesministerium für Bildung und Forschung (BMBF) Verbundprojekt Röntgenabsorptionsspektroskopie (05K10WMA und 05K10GU5), Deutsche Forschungsgemeinschaft (DFG) via SFB668 and by the Grant Agency of the Czech Republic (108/11/0853) is gratefully acknowledged.

*sven.bornemann@cup.uni-muenchen.de

¹K. Wildberger, V. S. Stepanyuk, P. Lang, R. Zeller, and P. H. Dederichs, *Phys. Rev. Lett.* **75**, 509 (1995).
²P. Gambardella, S. Rusponi, M. Veronese, S. S. Dhesi, C. Grazioli, A. Dallmeyer, I. Cabria, R. Zeller, P. H. Dederichs, K. Kern, C. Carbone, and H. Brune, *Science* **300**, 1130 (2003).
³O. Šipr, S. Bornemann, J. Minár, S. Polesya, V. Popescu, A. Simunek, and H. Ebert, *J. Phys.: Condens. Matter* **19**, 096203 (2007).
⁴P. Mavropoulos, S. Lounis, and S. Blügel, *Phys. Status Solidi B* **247**, 1187 (2010).
⁵A. Antal, B. Lazarovits, L. Udvardi, L. Szunyogh, B. Újfalussy, and P. Weinberger, *Phys. Rev. B* **77**, 174429 (2008).
⁶P. Ruiz-Díaz, R. Garibay-Alonso, J. Dorantes-Dávila, and G. M. Pastor, *Phys. Rev. B* **84**, 024431 (2011).
⁷S. Heinze, K. Bergmann, M. Menzel, J. Brede, A. Kubetzka, R. Wiesendanger, G. Bihlmayer, and S. Blügel, *Nat. Phys.* **7**, 713 (2011).
⁸S. Lounis, P. Mavropoulos, R. Zeller, P. H. Dederichs, and S. Blügel, *Phys. Rev. B* **75**, 174436 (2007).
⁹P. Ruiz-Díaz, J. L. Ricardo-Chávez, J. Dorantes-Dávila, and G. M. Pastor, *Phys. Rev. B* **81**, 224431 (2010).
¹⁰S. H. Vosko, L. Wilk, and M. Nusair, *Can. J. Phys.* **58**, 1200 (1980).
¹¹H. Ebert, D. Ködderitzsch, and J. Minár, *Rep. Prog. Phys.* **74**, 096501 (2011).
¹²R. Zeller, P. H. Dederichs, B. Újfalussy, L. Szunyogh, and P. Weinberger, *Phys. Rev. B* **52**, 8807 (1995).

¹³S. Bornemann, J. Minár, S. Polesya, S. Mankovsky, H. Ebert, and O. Šipr, *Phase Transitions* **78**, 701 (2005).
¹⁴O. Šipr, S. Bornemann, J. Minár, and H. Ebert, *Phys. Rev. B* **82**, 174414 (2010).
¹⁵V. P. Antropov, M. I. Katsnelson, B. N. Harmon, M. van Schilf-gaarde, and D. Kusnezov, *Phys. Rev. B* **54**, 1019 (1996).
¹⁶V. P. Antropov, M. I. Katsnelson, and A. I. Liechtenstein, *Physica B* **237-238**, 336 (1997).
¹⁷L. Udvardi, L. Szunyogh, K. Palotas, and P. Weinberger, *Phys. Rev. B* **68**, 104436 (2003).
¹⁸S. Bornemann, J. Minár, J. Braun, D. Ködderitzsch, and H. Ebert, *Solid State Commun.* **152**, 85 (2012).
¹⁹S. Mankovsky, S. Bornemann, J. Minár, S. Polesya, H. Ebert, J. B. Staunton, and A. I. Liechtenstein, *Phys. Rev. B* **80**, 014422 (2009).
²⁰J. B. Staunton, L. Szunyogh, A. Buruzs, B. L. Gyorffy, S. Ostanin, and L. Udvardi, *Phys. Rev. B* **74**, 144411 (2006).
²¹Š. Pick, V. S. Stepanyuk, A. N. Baranov, W. Hergert, and P. Bruno, *Phys. Rev. B* **68**, 104410 (2003).
²²P. Blonski and J. Hafner, *J. Phys.: Condens. Matter* **21**, 426001 (2009).
²³T. Balashov, T. Schuh, A. F. Takács, A. Ernst, S. Ostanin, J. Henk, I. Mertig, P. Bruno, T. Miyamachi, S. Suga, and W. Wulfhekel, *Phys. Rev. Lett.* **102**, 257203 (2009).
²⁴A. Mosca Conte, S. Fabris, and S. Baroni, *Phys. Rev. B* **78**, 014416 (2008).

- ²⁵G. Y. Guo and H. Ebert, *Phys. Rev. B* **51**, 12633 (1995).
- ²⁶R. Tyer, G. van der Laan, W. M. Temmerman, Z. Szotek, and H. Ebert, *Phys. Rev. B* **67**, 104409 (2003).
- ²⁷F. Wilhelm, P. Pouloupoulos, G. Ceballos, H. Wende, K. Baberschke, P. Srivastava, D. Benea, H. Ebert, M. Angelakeris, N. K. Flevaris, D. Niarchos, A. Rogalev, and N. B. Brookes, *Phys. Rev. Lett.* **85**, 413 (2000).
- ²⁸F. Wilhelm, P. Pouloupoulos, H. Wende, A. Scherz, K. Baberschke, M. Angelakeris, N. K. Flevaris, and A. Rogalev, *Phys. Rev. Lett.* **87**, 207202 (2001).
- ²⁹F. Wilhelm, M. Angelakeris, N. Jaouen, P. Pouloupoulos, E. T. Papaioannou, C. Mueller, P. Fumagalli, A. Rogalev, and N. K. Flevaris, *Phys. Rev. B* **69**, 220404 (2004).
- ³⁰V. V. Krishnamurthy, D. J. Singh, N. Kawamura, M. Suzuki, and T. Ishikawa, *Phys. Rev. B* **74**, 064411 (2006).
- ³¹M. M. Sigalas and D. A. Papaconstantopoulos, *Phys. Rev. B* **50**, 7255 (1994).
- ³²K. von Bergmann, S. Heinze, M. Bode, E. Y. Vedmedenko, G. Bihlmayer, S. Blügel, and R. Wiesendanger, *Phys. Rev. Lett.* **96**, 167203 (2006).
- ³³A. Deák, L. Szunyogh, and B. Ujfalussy, *Phys. Rev. B* **84**, 224413 (2011).
- ³⁴J. Honolka, T. Y. Lee, K. Kuhnke, D. Repetto, V. Sessi, P. Wahl, A. Buchsbaum, P. Varga, S. Gardonio, C. Carbone, S. R. Krishnakumar, P. Gambardella, M. Komelj, R. Singer, M. Fähnle, K. Fauth, G. Schütz, A. Enders, and K. Kern, *Phys. Rev. B* **79**, 104430 (2009).
- ³⁵V. Sessi, K. Kuhnke, J. Zhang, J. Honolka, K. Kern, A. Enders, P. Bencok, S. Bornemann, J. Minár, and H. Ebert, *Phys. Rev. B* **81**, 195403 (2010).
- ³⁶C. Etz, J. Zabloudil, P. Weinberger, and E. Y. Vedmedenko, *Phys. Rev. B* **77**, 184425 (2008).
- ³⁷B. Lazarovits, L. Szunyogh, and P. Weinberger, *Phys. Rev. B* **67**, 024415 (2003).
- ³⁸R. F. Sabiryanov, K. Cho, M. I. Larsson, W. D. Nix, and B. M. Clemens, *J. Magn. Magn. Mater.* **258–259**, 365 (2003).
- ³⁹B. Újfalussy, L. Szunyogh, P. Bruno, and P. Weinberger, *Phys. Rev. Lett.* **77**, 1805 (1996).
- ⁴⁰O. Šipr, J. Minár, and H. Ebert, *Cent. Eur. J. Phys.* **7**, 257 (2009).